Solar powered induction motor-driven water pump operating on a desert well, simulation and field tests

Abdel-Karim Daud[a,*], Marwan M. Mahmoud[b]

[a] Palestine Polytechnic University, P.O. Box 198, Hebron-West Bank, Israel
[b] An-Najah National University, P.O. Box 7, Nablus-West Bank, Israel

Received 21 November 2003; accepted 18 February 2004
Available online 23 November 2004

Abstract

A photovoltaic-powered water pumping system, employing an induction motor pump, capable of supplying a daily average of 50 m^3 at 37-m head has been developed. The system was installed on a desert well in Jordan, where: the average solar radiation amount to 5.5 kW h/m^3/day, to provide the Bedouins living in the well area with drinking water.

A mathematical model to enable testing the system performance by computer simulation was developed. This model allows the representation of motor torque in function of speed (and slip) at different supply frequencies, as well as the flow rate and efficiency of the system in function of supply frequency and pumping head.

Prior to its installation on the desert well, the system performance, in accordance with frequency and head, was thoroughly tested in the laboratory. As illustrated in this paper, simulation and laboratory testing results are well matched. At constant pumping head, the flow rate is proportional to the supply frequency of the motor. At constant flow rate, the pumping head is proportional to the supply frequency squared only in the range below the peak efficiency of the pump. For higher flow rate values, a special algorithm based on the experimental results could be developed.

Higher system efficiency is achievable at higher frequency. It is advisable to operate the motor pump at the nominal frequency, flow rate and head corresponding to maximum efficiency.

Long-term field testing of the system shows that it is reliable and has an overall efficiency exceeding 3%, which is comparable to the highest efficiencies reported elsewhere for solar powered pumps.

0960-1481/$ - see front matter © 2004 Elsevier Ltd. All rights reserved.
doi:10.1016/j.renene.2004.02.016

Keywords: Solar powered induction motor water pumps; Simulation of solar water pumping systems; Photovoltaic applications

1. Introduction

Powering of water pumping systems with photovoltaic generators (PV) has been an applied technology in many countries since 1977 [17].

The suitability of this technology for covering the daily water demands from wells in isolated areas had been established through many development projects implemented mostly in Africa, Asia and South America [1]. Thousands of systems operating at pumping heads in the range from 0 to 120 m have been successfully realized over the last 20 years.

Particularly in areas of average daily solar radiation intensity exceeding 5 kW h/m^3/day, medium water table depths in the range 15–60 m and of water requirements less than 100 m^3/day, PV systems had proven reliability and economic feasibility in comparison with diesel powered pumping systems [2]. In addition, these systems need very limited maintenance, since they operate without storage batteries and they do not pollute the environment.

Large number of papers on investigations in this field have been published in conferences and scientific journals. Most research attention had been paid to analysis of systems utilizing permanent magnet motors [3,4]. Systems utilizing three-phase induction motors were rarely analyzed in detail and it was mostly satisfied with the illustration of the testing results.

This paper reports on design, simulation testing and evaluation of a PV-powered pumping system utilizing induction motor. The system was designed to deliver a daily average of 50 m^3 at 37-m head from a desert well in Jordan. Besides developing a mathematical model for the system, the paper presents the results of computer simulation, laboratory tests and performance tests carried out while operating the system on the desert well.

2. System design and analysis

The PV-powered water pumping system investigated in this paper consists mainly of a PV generator, inverter, induction motor and a centrifugal pump (Fig. 1). The system was tested in a laboratory, then it was built on a desert deep well in Jordan, where it was tested under natural environmental conditions. Mathematical modeling of the system components, which is essential for testing the system through computer simulation and real measurements, was carried out as follows.

2.1. Centrifugal pump

Since the pump represents the mechanical load of the induction motor and its size identifies the power ratings of the other system components, including the necessary PV peak power, it is customary to start with its analysis. The utilized pump is a multistage centrifugal submersible one that can be characterized by the following

equations [5]

$$P_{\mathrm{p}} = 2.725 Q H \tag{1}$$

$$\eta_{\mathrm{p}} = \frac{P_{\mathrm{p}}}{P_{\mathrm{mech}}} \tag{2}$$

where P_{p} is the hydraulic output power of the pump in W, Q is the flow rate in m^3/h, H is the pumping head (total barometric head) in meters, η_{p} is the pump efficiency and P_{mech} is the input mechanical power of the pump.

Selection of the right pump for a specific discharge rate and a definite head occurs via the performance curves issued usually by the pump manufacturers. The curves illustrate Q in function of H and in function of η_{p}, while the stage number is a parameter [5]. For a constant flow rate, the higher the pumping head the higher should be the stage number and of course the associated input power.

Practically, for a definite head the maximum efficiency of the centrifugal pump varies according to flow rate in the range from 60 to 72% [5].

of magnetomotive force (or field) around the air gap. This field establishes a spatial distribution sinusoidal flux density in the air gap. The speed of rotation of the field is called the synchronous speed ($_s$ or n_s), which is defined by

$$_s 4\pi f/p \quad \text{or} \quad n_s = 120f/p \tag{3}$$

where f is the supply frequency and p is the number of poles [6–9]. A very useful quantity in studying induction machines is the slip s

$$s = \frac{_s -}{} = \frac{n_s - n}{n_s} \tag{4}$$

where or n is the speed of the rotor.

Per-phase equivalent circuit of a three-phase induction motor is shown in Fig. 2a [6–8]. An expression for the torque of an induction machine as a function of its slip may be obtained by application of Thevenin's theorem to the circuit model to the circuit model (Fig. 2b) [7]. The rotor circuit, as referred to the stator, may be considered as being attached to an equivalent Thevenin generator, as shown in Fig. 2b. Looking to the left into terminals 1 and 2, the open-circuit voltage will be that fraction of V_{ph} appearing across jX_m

$$V_{Th} = V_{ph} \frac{X_m}{\sqrt{R_1^2 + (X_1 + X_m)^2}} \tag{5}$$

The Thevenin generator impedance will be the impedance appearing at terminals 1 and 2 with the generator V_{ph} replaced by a short:

$$Z_{Th} = \frac{jX_m(R_1 + jX_1)}{R_1 + j(X_1 + X_m)} = R_{Th} + jX_{Th} \tag{6}$$

$$R_{Th} = \frac{R_1 X_m^2}{R_1^2 + (X_1 + X_m)^2} \quad \text{and} \quad X_{Th} = \frac{X_m[R_1^2 + X_1(X_1 + X_m)]}{R_1^2 + (X_1 + X_m)^2} \tag{7}$$

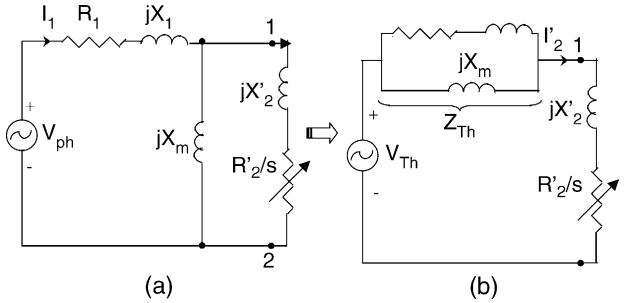

Fig. 2. (a) Equivalent circuit for one phase of a three-phase induction motor. (b) Application of Thevenin's theorem to the induction motor circuit model. V_{ph}, terminal phase voltage; V_{Th}, Thevenin voltage; R_1, stator resistance; X_1, stator reactance; X_m, magnetiting reactance; R'_2, rotor resistance referred to stator; X'_2, rotor reactance referred to stator; Z_{Th}, Thevenin impedance.

An expression for I'_2 may be written involving the Thevenin generator quantities:

$$I'_2 = \frac{V_{\mathrm{Th}}}{\sqrt{(R_{\mathrm{Th}} + R'_2/s)^2 + (X_{\mathrm{Th}} + X'_2)^2}} \tag{8}$$

Then, the electromagnetic torque of the motor is given by [6–9]:

$$T_{\mathrm{em}} = \frac{3}{s} I'^2_2 \frac{R'_2}{s} = \frac{3}{s} \frac{V^2_{\mathrm{Th}}(R'_2/s)}{(R_{\mathrm{Th}} + R'_2/s)^2 + (X_{\mathrm{Th}} + X'_2)^2} \tag{9}$$

Since by Eq. (5) V_{Th} is proportional to the voltage at motor terminals, note that at any speed the torque is proportional to square of the supply voltage.

There is a definite maximum torque $T_{\max}$ in the motor range of operation, called the breakdown torque, or pull-out torque, which is given by [6–9]:

$$T_{\max} = \frac{3}{2} \frac{V^2_{\mathrm{Th}}}{s \left(R_{\mathrm{Th}} + \sqrt{R^2_{\mathrm{Th}} + (X_{\mathrm{Th}} + X'_2)^2} \right)} \tag{10}$$

The speed of induction motors can be controlled by changing the supply frequency. But the terminal voltage can be considered proportional to the product of frequency and flux. If the voltage is maintained fixed at its rated value while the frequency is reduced below its rated value, the flux will increase. This would cause saturation of the air-gap flux. At low frequency, the reactances will decrease and the motor current may be too high. In order to avoid saturation and to minimize losses, motor is operated at rated air-gap flux by varying terminal voltage with frequency so as to maintain the ratio of voltage to frequency nearly constant or to maintain the breakdown torque constant [9,10,11,14].

If the frequency is increased above its rated value, the flux and torque would decrease. If the synchronous speed corresponding to the rated frequency f_n is called base speed $_{sn}$ or n_{sn}, the synchronous speed at any other frequency becomes

$$_s = k_o \; _{sn} \quad \text{or} \quad n_s = k_o n_{sn} \tag{11}$$

with

$$k_o = f/f_n \tag{12}$$

The expressions for R_{Th} and X_{Th} in Eq. (7) become:

$$R'_{\mathrm{Th}} = \frac{R_1 \left(\frac{X_{\mathrm{m}}}{f_n}\right)^2}{\left(\frac{R_1}{f}\right)^2 + \left(\frac{X_1 + X_{\mathrm{m}}}{f_n}\right)^2} \quad \text{and} \quad X'_{\mathrm{Th}} = f\left(\frac{X_{\mathrm{m}}}{f_n}\right) \frac{\left(\frac{R_1}{f}\right)^2 + \left(\frac{X_1}{f_n}\right)\left(\frac{X_1 + X_{\mathrm{m}}}{f_n}\right)}{\left(\frac{R_1}{f}\right)^2 + \left(\frac{X_1 + X_{\mathrm{m}}}{f_n}\right)^2} \tag{13}$$

Substituting Eqs. (5), (11)–(13) into Eq. (10), the line voltage (V_{L})-to-frequency (f) ratio k_{v} can be determined for a constant maximum torque by the following

equation

$$k_v = \sqrt{\frac{T_{\max}}{k_p}\left[\left(\frac{R_1}{f}\right)^2 + \left(\frac{X_1 + X_m}{f_n}\right)^2\right]\left[\frac{R'_{Th}}{f} + \sqrt{\left(\frac{R'_{Th}}{f}\right)^2 + \left(\frac{X'_{Th}}{f} + \frac{X'_2}{f_n}\right)^2}\right]}$$
$$\text{for } f < f_n = V_{LN}/f \quad \text{for } f \geq f \tag{14}$$

with

$$k_p = \frac{X_m^2}{2_{sn}} \tag{15}$$

where ($V_{LN} = \sqrt{3}V_{ph}$) is the rated line voltage of the motor.

Therefore, the torque expression in Eq. (9) becomes

$$T_{em} = 2k_p \frac{k_v^2}{\left(\frac{R_1}{f}\right)^2 + \left(\frac{X_1 + X_m}{f_n}\right)^2} \frac{(R'_2/sf)}{\left(\frac{sR'_{Th} + R'_2}{sf}\right)^2 + \left(\frac{X'_{Th}}{f} + \frac{X'_2}{f_n}\right)^2} \tag{16}$$

T_{em} is also called the torque developed by electromagnetic energy conversion process between the stator and rotor of the motor. Therefore, the electromagnetic power is defined as follows [12,13]

$$P_{em} = T_{em} = k_{o\ sn}(1 - s)T_{em} = P_{mech} + P_{LK} \tag{17}$$

where P_{mech} is the mechanical output power and P_{LK} is the constant loss (mostly rotational losses). Substituting T_{em} from Eq. (16) into Eq. (17), the slip s can be determined by the roots of the following quadratic equation

$$k_1 s^2 + k_2 s + R_l^2 = 0 \tag{18}$$

$$s = \frac{-k_2 - \sqrt{k_2^2 - 4k_1 R_l^2}}{2k_1} \tag{19}$$

with

$$k_{10} = \frac{k_v^2}{(R_1/f)^2 + ((X_1 + X_m)/f_n)^2}; \quad k_{20} = \left(\frac{X'_{Th}}{f} + \frac{X_m}{f_n}\right)^2;$$
$$k_{30} = \frac{2k_p k_{10} R'_{2\ sn}}{f_n P_{em}}; \quad k_1 = R_{l2}^{Th} + (k_{20} + k_{30})f^2; \quad k_2 = 2R'_{Th}R'_2 - k_{30}f^2. \tag{20}$$

From the circuit model in Fig. 2a and by using Eq. (12), the equivalent input impedance (Z_{in}) is given by

$$Z_{in} = R_1 + jk_oX_1 + jk_oX_m//(R_2'/s + jk_oX_2') = R_{in} + jX_{in} = |Z_{in}| < \varphi \tag{21}$$

with

$$R_{in} = R_1 + \frac{k_o^2X_m^2(R_2'/s)}{(R_2'/s)^2 + k_o^2(X_2' + X_m)^2};$$
$$X_{in} = k_oX_1 + k_oX_m\frac{(R_2'/s)^2 + k_o^2X_2'(X_2' + X_m)}{(R_2'/s)^2 + k_o^2(X_2' + X_m)^2}; \quad \varphi = \tan^{-1}(X_{in}/R_{in}) \tag{22}$$

The line stator current (I_{1L}) can be calculated by:

$$I_{1L} = V_{ph}/|Z_{in}| \tag{23}$$

The input electrical power of the motor (P_{in}) is given by:

$$P_{in} = \sqrt{3}V_LI_{1L}\cos\varphi \tag{24}$$

Therefore, the motor efficiency is defined as:

$$\eta_m = \frac{P_{mech}}{P_{in}} \tag{25}$$

2.3. Inverter

The inverter in Fig. 1 is used to convert the dc voltage into three-phase ac voltage to supply the induction motor driving the pump. The output voltage of the inverter is sinusoidal with variable amplitude and frequency.

The output is usually controlled by a pulse-width modulation (PWM) control circuit forcing the voltage frequency ratio to remain constant [14]. The input voltage of the inverter produced by the PV generator fluctuates according to solar radiation level and ambient temperature, which results in variation of the output voltage and frequency. However, the inverter starts delivering power to the induction motor when its output frequency and voltage achieve 30 Hz and about 60% of the nominal voltage value, respectively.

The efficiency of the inverter (η_i) ranges from 80 to 90% and is defined as

$$\eta_i = \frac{P_{in}}{P_{dc}} \tag{26}$$

where P_{dc} is the output power of the generator.

2.4. P_V generator

The PV generator converts the solar radiation falling down on its surface into electric dc power, which is converted to ac power by the inverter to supply the induction motor. It consists of a number of PV modules connected in series, building a row to generate dc

voltage suitable to the inverter input, and a number of rows connected in parallel to generate the power (P_{dc}) necessary to run the pumping system [15].

The efficiency of the PV generator (η_{pv}) is obtainable as

$$\eta_{pv} = \frac{P_{dc}}{A_{pv} G} \tag{27}$$

where A_{pv} is the surface area of the PV generator in m^2 and G is the solar radiation intensity in W/m^2. According to PV type, the maximum value of η_{pv} varies from 8 to 14%.

Respecting the standard conditions [17], the PV peak power (P_{dc}) is computed as

$$P_{dc} = \frac{E_{dc}}{PSH} \tag{28}$$

where E_{dc} (in kW h) is the total daily energy required from the PV generator to operate the pumping system and PSH is the peak number of sun hours on the site of the system.

To account for the effect of temperature, dust, variation of solar radiation and resistive losses on the output power produced by the PV generator, it is necessary to multiply the value obtained for P_{dc} Eq. (28) with a safety factor amounting to 1.3 [15,17].

The overall system efficiency (η_T), which is the ratio of output hydraulic power to the input solar power, is computable as:

$$\eta_T = \eta_P \eta_m \eta_i \eta_{pv} \tag{29}$$

Properly designed, specified and PV pumping system have an overall efficiency in the range from 3 to 4.5%.

3. Performance tests, results and discussion

According to the design shown in Fig. 1 and illustrated sizing method, a PV-powered water pumping system was designed to meet the water requirements on a desert well site in Jordan amounting in average to 50 m^3/day. The static water level of the well is 5 m, while the dynamic water level is 30 m at an output of 19 m^3/day. The height of the storage tank is 5 m which means that the total pumping head, including friction losses, is 37 m. The climatologically data of Jordan are obtained from Ref. [16].

Considering a daily average of solar radiation intensity on the well site amounting to 5.5 kW h/m^2/day, the described sizing method resulted in the component specifications illustrated in Table 1.

Table 1
Component specifications

Component	Input voltage	Output voltage	Output power (W)
PV generator		230 V DC	2800 (peak)
Inverter	230 V DC	3–127 V AC	3000
Motor-pump set	3–127 V AC		1100

Table 2
The motor losses in function of the supply frequency

f/Hz	30	35	40	45	50	55
P_{LK}/W	87.7	102.6	117.2	130.2	145	160.7

3.1. Simulation and laboratory tests

Considering the rated parameter values of the selected induction motor

$$n = 2835 \text{ rpm}; \quad P_n = 1100 \text{ W}; \quad V_n = 127 \text{ V}_{ac}; \quad R_1 = R_2' = 1.72\ \Omega;$$
$$X_1 = X_2' = 3.860\ \Omega; \quad X_m = 60\ \Omega$$

we obtain by Eq. (17), the motor losses in function of the supply frequency as shown in Table 2.

Substituting the outlined motor parameters in the developed mathematical model, we obtain through simulation the motor torque as a function of speed (and slip) for different supply frequencies as shown in Fig. 3. For a constant (V/f) ratio, the motor develops a constant maximum torque, except at low speeds (or frequencies). The motor, therefore, operates in constant torque mode [6,7,9,10]. The maximum torque will have lower value for low frequencies (or speeds) due to stator resistance drop. When it is required that the same maximum torque at low speeds, (V/f) ratio is increased at frequencies. When either V saturates or reaches rated value at rated speed, it, cannot be increased with frequency in order to maintain a constant (V/f) ratio. Therefore, above rated speed, frequency is changed with V maintained constant, giving a constant power operation and a reduction in the maximum torque with increase in frequency as shown in Fig. 3.

The above-specified motor-pump set were exposed to laboratory performance tests before installing them within the pumping system on the desert well. The PV generator was represented in a rectifier with controllable output voltage and power.

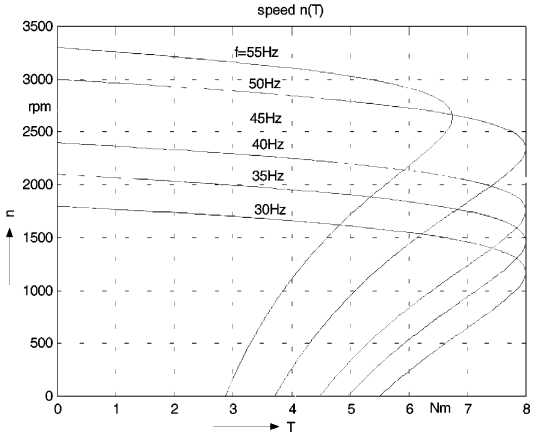

Fig. 3. Simulation results for the used induction motor; torque as a function of speed (and slip) with the supply frequency as parameter.

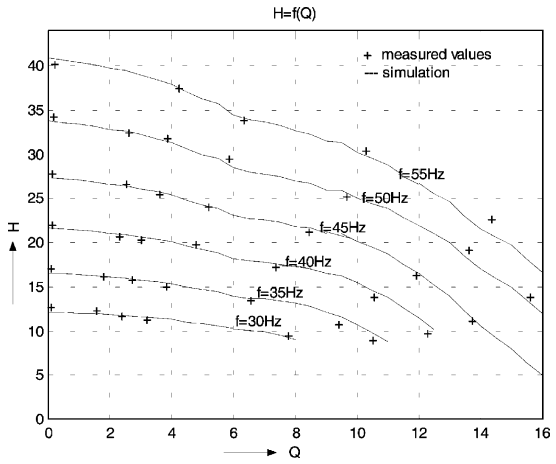

Fig. 4. Simulation and laboratory measurement results for the used inverter–motor-pump set, the flow rate ($\dot{Q}$ in m^3/h) as a function of head (H in m) with the supply frequency f as parameter.

The motor pump was submerged in a water tank, where the pumping head (adjustable) could be simulated by means of controllable valves.

The output of inverter is also controllable, where the voltage frequency ratio remains constant. So this pump test stand allows the measurement of all performance curves required for characterizing the pumping system. Fig. 4 illustrates the simulation and measuring results of the flow rate ($\dot{Q}$) in function of pumping head (H), whereby the supply frequency (f) is a parameter, i.e. each curve belongs to a constant rpm value of the pump. It is clear that simulation and measuring results are well matched. Usually, pump manufacturers offer a curve for only the nominal frequency.

For the simulation program, the 50 Hz curve $H = f(Q)$ was needed from the data sheet of the manufacturer to be stored in the pump-data file.

Based on practical experiments in the laboratory, the algorithms below are developed to calculate $H = f(Q)$

$$\frac{H}{H} = \left(\frac{f}{f_n}\right)^2 \quad \text{for } \dot{Q} \le \dot{Q}_{\eta\max} \tag{30}$$

$$\frac{H}{H} = \left[1 \pm \left(\frac{\dot{Q} - \dot{Q}_{\eta\max}}{\dot{Q}_{\eta\max}}\right)^2\right]\left(\frac{f}{f_n}\right)^2 \quad \text{for } \dot{Q} > \dot{Q}_{\eta\max} \tag{31}$$

where

$$\dot{Q}_{\eta\max} = \dot{Q}_{nl\ \eta\max}\left(\frac{f}{f_n}\right); \quad \dot{Q}_{nl\ \eta\max} = \dot{Q} \text{ at } f_n$$

$$= 50 \text{ Hz} \quad \text{and} \quad \eta_{\max} \quad (+ \text{ for } f > f_n \text{ and } - \text{ for } f < f_n)$$

Generally, one has to be careful to operate the pump as closely as possible to the nominal operating point, specified by the manufacturer, to get maximum efficiency.

At constant , it should be noted in Fig. 4 that increasing of f cause high rising of , which is proportional to the input power. On other hand, at constant higher is possible by increasing of f. Fig. 5 illustrates the measured subsystem efficiency (η) in function of (i.e. inverter

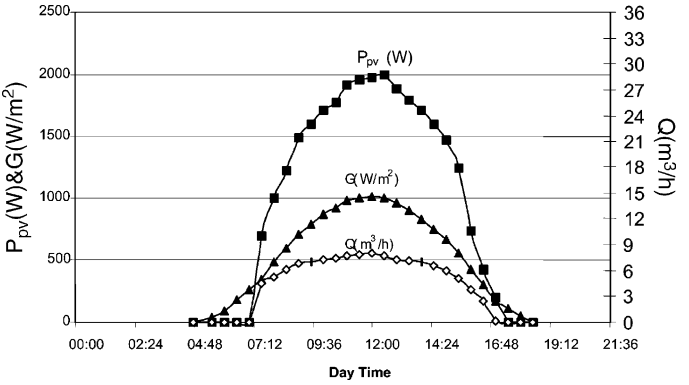

Fig. 7. Measurement results of G, P_{pv} and Q in function of day hours (T) for the complete PV-powered water pumping system operating on a desert well in Jordan.

3.2. Testing the pumping system on a desert well

After testing the inverter–motor-pump set in the laboratory, it was built with a PV generator according to Fig. 1 on the previously specified desert well, to provide the inhabitants on the well site with drinking water. With respect to the well data, the daily water demand and the average solar radiation on the well site, the peak power of the PV generator was determined according to Eq. (28) as 2800 W.

It consists of 4 PV strings connected in parallel and each string consists of 14 PV modules connected in series. At maximum power point [17], this generator provides the inverter with 230 V_{dc}, whereby the inverter provides the motor with 127 V_{ac} (three phase, 50 Hz).

This pumping system was exposed to continuous computer-supported measurements for 1 year. Fig. 7 illustrates the obtained measuring results for a clear sunny day in July, where G proceeds almost sinusoidally

$$G(t) = G_{\max} \sin \frac{\pi}{T} t \tag{32}$$

$$G_{\text{av}} = \frac{1}{T} \int_0^T G_{\max} \sin \frac{\pi}{T} t \, \mathrm{d}t \tag{33}$$

where $G_{\max}$ and G_{av} are maximum and daily average values, respectively, of solar radiation, while T is the length of solar day in hours. Applying Eq. (33) on the measured solar radiation curve in Fig. 7, we obtain:

$$G_{\text{av}} = \frac{1}{12.5} \int_0^{12.5} 1000 \sin \frac{\pi}{12.5} t \, \mathrm{d}t = 636.62 \text{ W/m}^2$$

The total daily solar energy intensity (E_{sr}) is now computable as:

$$E_{\text{sr}} = G_{\text{av}} T = 636.25 \times 12.5 = 7957.75 \text{ W h/m}^2 \tag{34}$$

With respect to the measured output power curve of the PV generator (P_{pv}) and the total area of the 40 cells ($10\times10\ cm^2$) constituting each of the 56 PV modules, we obtain according to Eq. (27): $\eta_{pv}=8.93\%$.

The sinking of η_{pv} refers to the resistive losses and to the high PV cell temperature amounting to about 70 °C during the main day hours. η_{pv} achieved 10.4% in days of lower ambient temperature.

Integrating the measured water flow rate curve in Fig. 7 yields the total daily water capacity pumped by the system

$$\int_7^{18} Q\,dt = 63.5\ m^3/day$$

whereby the daily total system efficiency is computed according to Eq. (29) as $\eta_T=3.09\%$.

It should be noted that $\eta_T=3.1\%$ at peak solar radiation, which means that it remains almost constant during the main sunshine hours (8–15 h). At higher PV efficiency, e.g. $\eta_{pv}=10.4\%$ a total efficiency of $\eta_T=3.61\%$ was measured.

Based on the above results, the efficiency of the inverter–motor-pump set is 34.72%, while the efficiency of the motor-pump amount to 36.94%, since the inverter efficiency was separately measured to $\eta_T=94\%$.

Based on 1-year measurements via data acquisition system, where an annual solar energy intensity on the well site of 2033 kW h/m^3/year had been registered, the pumping system had delivered 1985 m^3/year.

This amount corresponds to an average of 54.4 m^3/day which is very close to the design criteria. In comparison to diesel powered water pumping systems used usually in such remote areas of Jordan, the water costs of PV-powered systems amount to only 0.62 of water costs pumped by diesel [2].

4. Conclusions

The developed mathematical model allows, through simulation, the analysis of PV-powered water pumping system driven by an induction motor. Simulation and laboratory testing results are well matched.

At constant flow rate (Q) the variation of pumping head (H) is proportional to the supply frequency squared only in the range below the flow rate value corresponding to the peak efficiency of the pump (Eq. (30)). At higher flow rate range, it applies the algorithm (Eq. (31)), which we developed from the laboratory measurements.

At constant pumping head higher system efficiency is achievable at higher supply frequency. It is advisable to operate the pump as far as possible at the flow rate and head corresponding to the maximum efficiency given by the manufacturer.

The reliability of the used design method for the PV-powered pumping system is verified through simulation tests and long-term field tests under natural environmental conditions.

References

[1] Halcrow W. Hand book on solar water pumping. UNDP Project GLO/80/003, World Bank, United Nations. UK: Reading; 1984.
[2] Mahmoud MM. Experience results and techno-economic feasibility of using photovoltaic generators instead of diesel motors for water pumping from rural desert wells in Jordan. IEE Proc 1990;137:Pt C(6).
[3] van Overstraeten R, Mertens R, Kerbeche T, Anis W. Analysis for water pumping systems. Solar Wind Technol 1984;1(4).
[4] Pulfrey DL, Ward PRB, Dunford WG. A powered system for medium-head pumping. Solar Energy 1987; 38(4).
[5] KSB-Pump catalogue issued 1/1/1998, Frankenthal-Germany.
[6] Chapman SJ. Electric machinery fundamentals. New York: McGraw-Hill; 1991.
[7] McPherson G, Laramore RD. An introduction to electric machines and transformers. New York: Wiley; 1990.
[8] Müller G. Elektrische Maschinen, Grundlagen, Aufbau und Wirkungsweise. Berlin: VEB Verlag Technik; 1982.
[9] Dubey GK. Fundamentals of electrical drives. Narosa Publishing House; 1995.
[10] Leonhard W. Control of electrical drives. Berlin: Springer; 1990.
[11] Dietrich D, Konhäuser W. Mikrocomputer-geregelte Asynchron-maschinen. R. Oldenbourg Verlag GmbH; 1986.
[12] Hindmarsch J. Electrical machines and their applications, 4th ed. New York: Pergamon Press; 1984.
[13] Hindmarsch J. Electrical machines and drives, worked examples, 2nd ed. New York: Pergamon Press; 1985.
[14] Rashid MH. Power electronics. Englewood, Cliffs, NJ: Prentice-Hall; 1993.
[15] Mahmoud MM. Jordan's first photovoltaic water pumping system. Proceedings of the international seminar on appropriate technology in the fields of solar and wind energy applications. Amman, Jordan: Royal Scientific Society; 1987.
[16] Mahmoud MM, Nabhan I. Determination of optimum tilt angle of single and multi rows of photovoltaic arrays for selected sites in Jordan. Solar Wind Technol 1990;7:6.
[17] Buresch M. Photovoltaic energy systems. New York: McGraw-Hill; 1983.